Detecting Burnscar from Hyperspectral Imagery via Sparse Representation with Low-Rank Interference

Minh Dao[1], Xiang Xiang[1], Bulent Ayhan[2], Chiman Kwan[2], Trac D. Tran[1]
Johns Hopkins Univeristy, 3400 N. Charles St, Baltimore, MD 21218, USA
Applied Research LLC, 9605 Medical Center Dr., Rockville, MD 20850, USA

1 Introduction

1.1 Sparse Representation

For the last several years, sparse signal representations have proven to be extremely powerful tools in solving many signal processing, computer vision and pattern recognition problems. These applications mainly rely on the observation that given signals are normally well described by low-dimensional subspaces of some proper bases or dictionaries. According to sparse representation theory, an unknown signal $\boldsymbol{s} \in \mathbb{R}^N$ in the linear representation of columns of a dictionary matrix $\boldsymbol{D} \in \mathbb{R}^{M \times N}$ can be faithfully recovered from the measurements $\boldsymbol{y} \in \mathbb{R}^M$ (M $\ll$ N) if $\boldsymbol{s}$ is sparse i.e. it contains significantly fewer measurements than the ambient dimension of the signal. The reconstruction of $\boldsymbol{s}$ is solved by the following sparsity-driven l_1-based linear programming problem [1,2]:

$$\min_{\boldsymbol{s}} \|\boldsymbol{s}\|_1 \quad s.t.\ \boldsymbol{y} = \boldsymbol{D}\boldsymbol{s}$$

where the l_1-norm is defined as $\|\boldsymbol{s}\|_1 = \sum_{i=1}^{N} s_i$ with s_i's being the entries of $\boldsymbol{s}$.

For multiple measurements $\boldsymbol{Y} = [\boldsymbol{y}_1|\boldsymbol{y}_2|\ ...\ |\boldsymbol{y}_K]$ capturing similar events, the inter-correlation between observations in the sparse representation can be further reinforced by incorporating them to share the same sparsity patterns of the sparse coefficients. The sparse coefficients of the measurements can be recovered jointly by solving the a l_{12}-norm regularized minimization [3]:

$$\min_{\boldsymbol{S}} \|\boldsymbol{S}\|_{1,2} \quad s.t.\ \boldsymbol{Y} = \boldsymbol{D}\boldsymbol{S}$$

where the norm $\|\boldsymbol{S}\|_{1,2}$ is defined as the sum of the l_2-norm of rows of $\boldsymbol{S}$. In other words, we first apply l_2-norm on each row to enforce the 'joint' effect and then apply l_1-norm on the resulting vector to enforce the 'sparsity'; which promotes a matrix $\boldsymbol{S}$ with row-sparse property.

1.2 Low-rank Matrix Recovery

Matrix completion [4] and robust principal component analysis (Robust PCA or RPCA) [5,6] are two highly applicable low-rank matrix recovery techniques in which matrix completion retrieves missing information of the data while RPCA recovers an underlying low-rank structure from its sparse but grossly corrupted entries. The two problems have been beneficial in solving a number of applications including background modeling, target tracking [5] and image alignment [6].

In the most general form, low-rank matrix recovery problem consists of recovering a low-rank matrix $\boldsymbol{X} \in \mathbb{R}^{N_1 \times N_2}$ from a set of M linear measurements: $\boldsymbol{y} = \mathcal{A}(\boldsymbol{X})$ where $\mathcal{A}: \mathbb{R}^{N_1 \times N_2} \rightarrow \mathbb{R}^M$ is a linear map. To recover $\boldsymbol{X}$, we find the simplest model that fits the low-rank observations by

$$\min_{\boldsymbol{X}} rank(\boldsymbol{X}) \quad s.t.\ \boldsymbol{Y} = \mathcal{A}(\boldsymbol{X})$$

The above rank-minimization problem is a non-convex and intractable problem. Under some mild conditions [4], however, the rank-minimization problem can be relaxed to the convex problem of nuclear norm minimization:

$$\min_{\boldsymbol{X}} \|\boldsymbol{X}\|_* \quad s.t.\ \boldsymbol{Y} = \mathcal{A}(\boldsymbol{X})$$

where the nuclear matrix norm $\|\boldsymbol{X}\|_*$ is defined as sum of all singular values of the matrix $\boldsymbol{X}$.

A highly applicable subset of low-rank matrix recovery problems is the matrix completion problem where the goal is to recover an unknown matrix from a subset of its entries. Typically, given an incomplete observation matrix $\boldsymbol{Y} = \boldsymbol{X}|_\Omega$, where Ω is the index set of available entries of $\boldsymbol{X}$, we want to recover back the original matrix $\boldsymbol{X}$ with the prior knowledge that $\boldsymbol{X}$ is low-rank. Here, $\mathcal{A}$ is the linear operator that sets unobserved entries to zero. Again, to achieve $\boldsymbol{X}$, a nuclear norm minimization is proposed as follows [4]:

$$\min_{\boldsymbol{X}} \|\boldsymbol{X}\|_* \quad s.t.\ \boldsymbol{Y} = \boldsymbol{X}|_\Omega$$

Another recent landmark result introduced by Candes et al investigates the problem of robust principal component analysis (RPCA) [5]. The question is how to efficiently recover a low-rank structure $\boldsymbol{X}$ from the corrupted observed version $\boldsymbol{Y} = \boldsymbol{X} + \boldsymbol{E}$, where $\boldsymbol{E}$ is a sparse matrix which contains most of zero or near-zero entries but the other magnitudes can be arbitrarily large. To separate $\boldsymbol{X}$ and $\boldsymbol{E}$, a principle component pursuit strategy is proposed [5]:

$$\min_{\boldsymbol{X}} \|\boldsymbol{X}\|_* + \lambda\|\boldsymbol{E}\|_1 \quad s.t. \boldsymbol{Y} = \boldsymbol{X} + \boldsymbol{E}$$

where λ is a positive weighting parameter, and $\|\cdot\|_1$ is the l_1-norm of a matrix. This problem in some sense can be viewed as a generalization of matrix completion. In fact, if we set entries of $\boldsymbol{E}$ such that $\boldsymbol{E}_{ij} = -\boldsymbol{X}_{ij}$ with $(i,j) \in \Omega$, then RPCA turns into the matrix completion problem.

2 Burnscar Detection for Hyperspectral Imagery

In this section, we propose a burnscar detection model for hyperspectral imaging (HSI) data. The proposed model contains two-processing steps in which the first step separate and then suppress the cloud information presenting in the data set using an RPCA algorithm and the second step detect the burnscar area in the low-rank component output of the first step.

2.1 Cloud separation and suppression via robust PCA

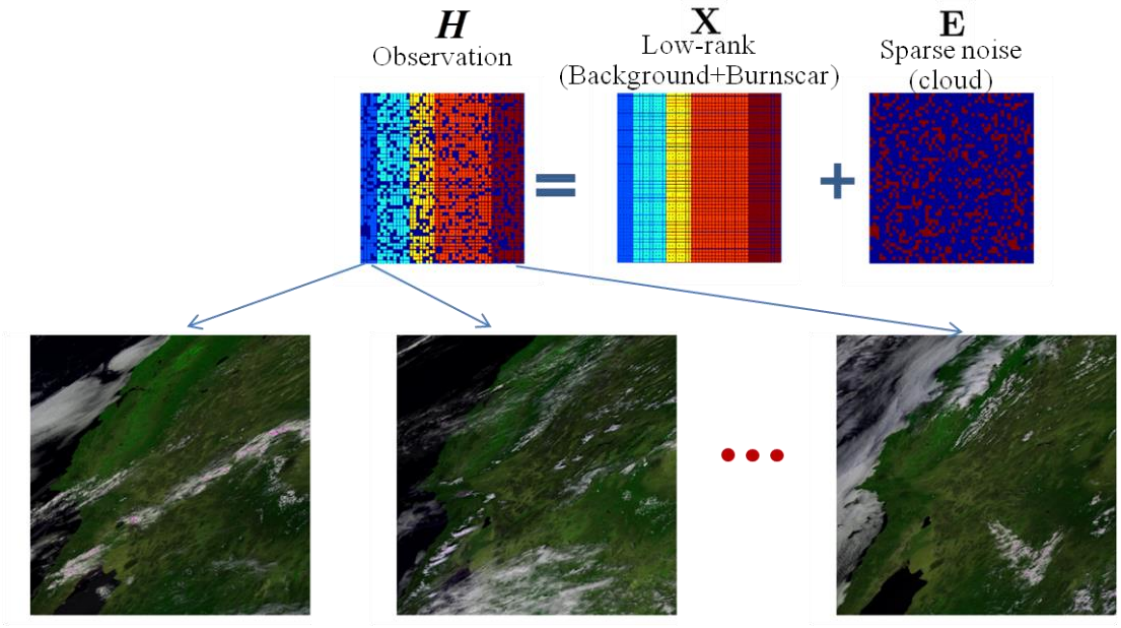

Fig. 1. Cloud suppression via robust PCA.

As discussed in section 1, RPCA has the capability of decomposing a matrix into an underlying low-rank structure and a sparse component. In the first step, we apply this idea to separate the cloud information from the processing HSI data. In the testing data set, each of the hyperspectral frames contains three main components of interest: the background content, the burning area and the cloud information. The background content of hyperspectral frames stays almost stationary while the burning area is also stable in consecutive days, hence the background-plus-burning content in each frame should be a low-rank component over time. Furthermore, the cloud information is changing very fast and may look completely different from any two consecutive days. Therefore, by vectorizing each spectral band of consecutive frames and concatenating into a big matrix $\boldsymbol{H}$ (i.e., each seven columns of $\boldsymbol{H}$ are the seven bands of each hyperspectral frame in vector forms), $\boldsymbol{H}$ can be decomposed into a low-rank matrix $\boldsymbol{X}$ and a sparse component $\boldsymbol{E}$ using the RPCA algorithm where $\boldsymbol{X}$ contains the background-plus-burning information while $\boldsymbol{E}$ captures all cloud content (Fig. 1). Matrix $\boldsymbol{X}$ is then used as the input of the detection step to determine the burning area while $\boldsymbol{E}$ can be utilized to decide the area that cloud presents as well as the cloud level presenting in every pixel (which may be used to robustify the detection step).

2.2 Burnscar Detection via Sparsity-based Representation

After suppressing the cloud information in every hyperspectral frame, the next step is to automatically classify every pixel if it belongs to a burnscar or non-burnscar area using a sparsity-based representation model. Furthermore, we robustify the target detection performance via a spatial-temporal joint sparsity model which derives from the observation that neighborhood pixels from the same hyperspectral image as well as previous and next hyperspectral frames usually have similar spectral characteristics. Thus, by representing nearby pixels simultaneously in a batch processing, we can bring another level of robustness into the burnscar detection result.

The HSI sparsity model is based on the assumption that the spectral characteristic of each pixel approximately lies in the low-dimensional subspace that is spanned by the training samples of the same class presenting in that pixel. Let $\boldsymbol{y} \in \mathbb{R}^M$ be an HSI pixel staying in M spectral bands and the entries of $\boldsymbol{y}$ are correspondent with the spectral bands. If the pixel $\boldsymbol{y}$ is a background, it lies in a low-dimensional subspace domain of the training background $\boldsymbol{D}_B = \{\boldsymbol{d}_B^i\}_{i=1,2,\dots,N_B}$ and the approximated representation of $\boldsymbol{y}$ is the sparse linear combination of these samples:

$$\mathbf{y} = \sum_{i=1}^{N_B} s_B^i \mathbf{d}_B^i = \underbrace{\left[\mathbf{d}_B^1, ..., \mathbf{d}_B^{N_B}\right]}_{\mathbf{D}_B} \underbrace{\begin{bmatrix} s_B^1 \\ ... \\ s_B^{N_B} \end{bmatrix}}_{\mathbf{s}_B} = \mathbf{D}_B \mathbf{s}_B$$

where the matrix $\boldsymbol{D}_B$ is the training background dictionary which is adaptively taken from the local neighborhood of the processing pixel, and the coefficient vector $\boldsymbol{s}_B$ should be sparse in term that only a few elements of $\boldsymbol{s}_B$ are nonzero.

If the pixel $\boldsymbol{y}$ is a burning pixel, containing no information of the background, the representation of its spectrum lies in a sparsity spanning of the training target samples $\boldsymbol{D}_C = \{\boldsymbol{d}_C^i\}_{i=1,2,\dots,N_C}$:

$$\mathbf{y} = \sum_{i=1}^{N_C} s_C^i \mathbf{d}_C^i = \underbrace{\left[\mathbf{d}_C^1, ..., \mathbf{d}_C^{N_c}\right]}_{\mathbf{D}_C} \underbrace{\begin{bmatrix} s_C^1 \\ ... \\ s_C^{N_C} \end{bmatrix}}_{\mathbf{s}_C} = \mathbf{D}_C \mathbf{s}_C$$

where we construct the target dictionary $\boldsymbol{D}_C$ by taking all burning pixels of an reference HSI frame that contains no cloud information in the burning area. Therefore, an observed sample $\boldsymbol{y}$ being a union of the background and target samples stays in a sparse domain of the combining dictionary $\boldsymbol{D}_B$ and $\boldsymbol{D}_C$ and can be compactly represented as:

$$\mathbf{y} = \underbrace{\begin{bmatrix} \mathbf{D}_C & \mathbf{D}_B \end{bmatrix}}_{\mathbf{D}} \underbrace{\begin{bmatrix} \mathbf{s}_C \\ \mathbf{s}_B \end{bmatrix}}_{\mathbf{s}} = \mathbf{D}\mathbf{s}$$

Once the sparse solution $\boldsymbol{s}$ is obtained, the class label is decided by comparing the residuals with respect to the background and target dictionaries, where the residual of the target dictionary is $r_C = \|\boldsymbol{y} - \boldsymbol{D}_C\boldsymbol{s}_C\|$ and the residual of the background component is $r_B = \|\boldsymbol{y} - \boldsymbol{D}_B\boldsymbol{s}_B\|$. Specifically in our work, we compare the difference or ratio between these two residuals to determine the detected area of the burning pixels.

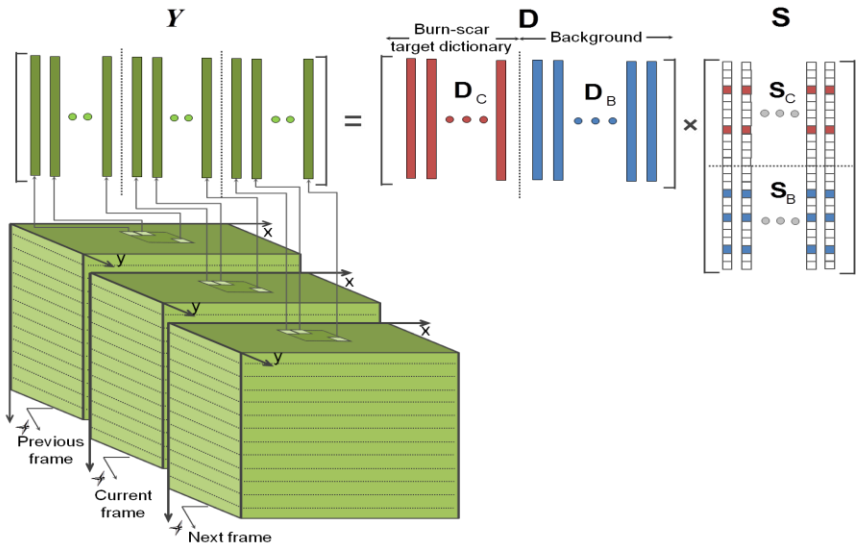

Fig. 2. Hyperspectral burning detection via joint-sparsity model.

With the observation that small neighborhood HSI pixels usually belong to the same materials, we further propose a joint sparsity model by enforcing them to have the same sparsity support of the training samples. If an observed pixel is defined as background, it is very likely that the nearby pixels in the same frame are also defined as background and should belong to the same class of materials as the testing observation. Not only that, the pixels at the same locations in the previous and next frames should also share the same materials. Moreover, the area that a burn appears should also smooth. Consequently, if an observed pixel is supposed to be in a burning area, the pixels in its small neighborhood in both spatial and time domain should also be classified as being burned. Therefore, they can be approximated by a linear sparse combination from the same few samples in the target-background dictionary $\boldsymbol{D}$. The joint sparsity structure for the burnscar detection is formulated as follows:

$$\begin{aligned} \mathbf{Y} &= \begin{bmatrix} \mathbf{y}_1 & \mathbf{y}_2 & \cdots & \mathbf{y}_{3N^2} \end{bmatrix} \\ &= \begin{bmatrix} \mathbf{D}_C & \mathbf{D}_B \end{bmatrix} \begin{bmatrix} \mathbf{s}_{C_1} & \mathbf{s}_{C_2} & \cdots & \mathbf{s}_{C_{3N^2}} \\ \mathbf{s}_{B_1} & \mathbf{s}_{B_2} & \cdots & \mathbf{s}_{B_{3N^2}} \end{bmatrix} \\ &= \underbrace{\begin{bmatrix} \mathbf{D}_C & \mathbf{D}_B \end{bmatrix}}_{\mathbf{D}} \underbrace{\begin{bmatrix} \mathbf{S}_C \\ \mathbf{S}_B \end{bmatrix}}_{\mathbf{S}} = \mathbf{D}\mathbf{S} \end{aligned}$$

3 Experimetal Results

All experiments are conducted on the public MODIS dataset available at NASA official website.

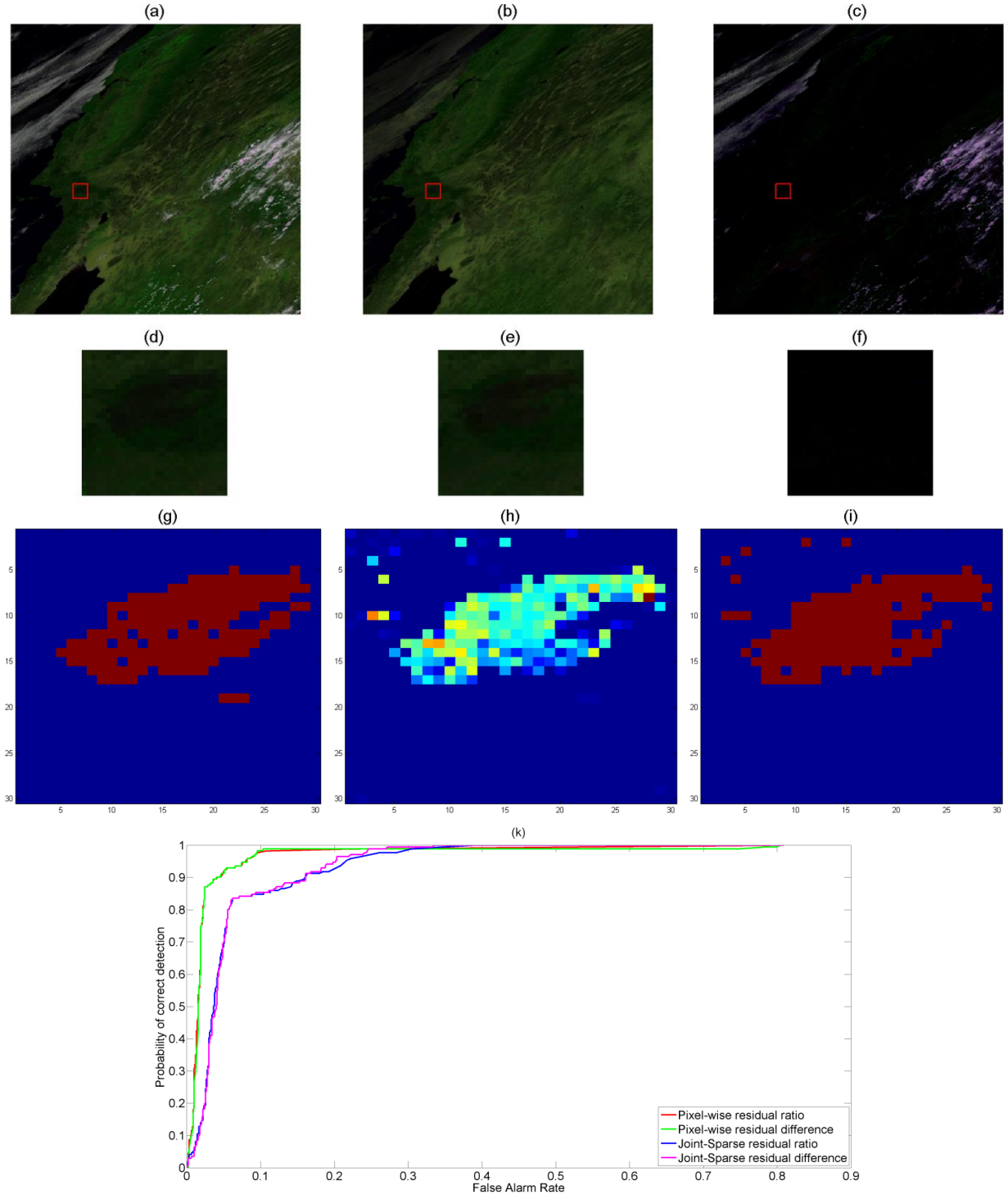

Fig. 3: Burnscar detection result for frame A2009252 (almost no cloud): (a) Original HSI image in RGB mode; (b) Output low-rank component of RPCA; (c) Output sparse component of RPCA (cloud); (d) (e) and (f) Zoom-in patches of HSI images within the burnscar testing region (red-rectangle region) shown in (a), (b) and (c), respectively; (g) ground truth burn map within the testing patch; (h) Output residual difference of joint-sparsity detection; (i) Output burnscar

detection (by thresholding (h)); the receiver operating characteristic (ROC) curves of pixel-wise and joint-sparsity target detections.

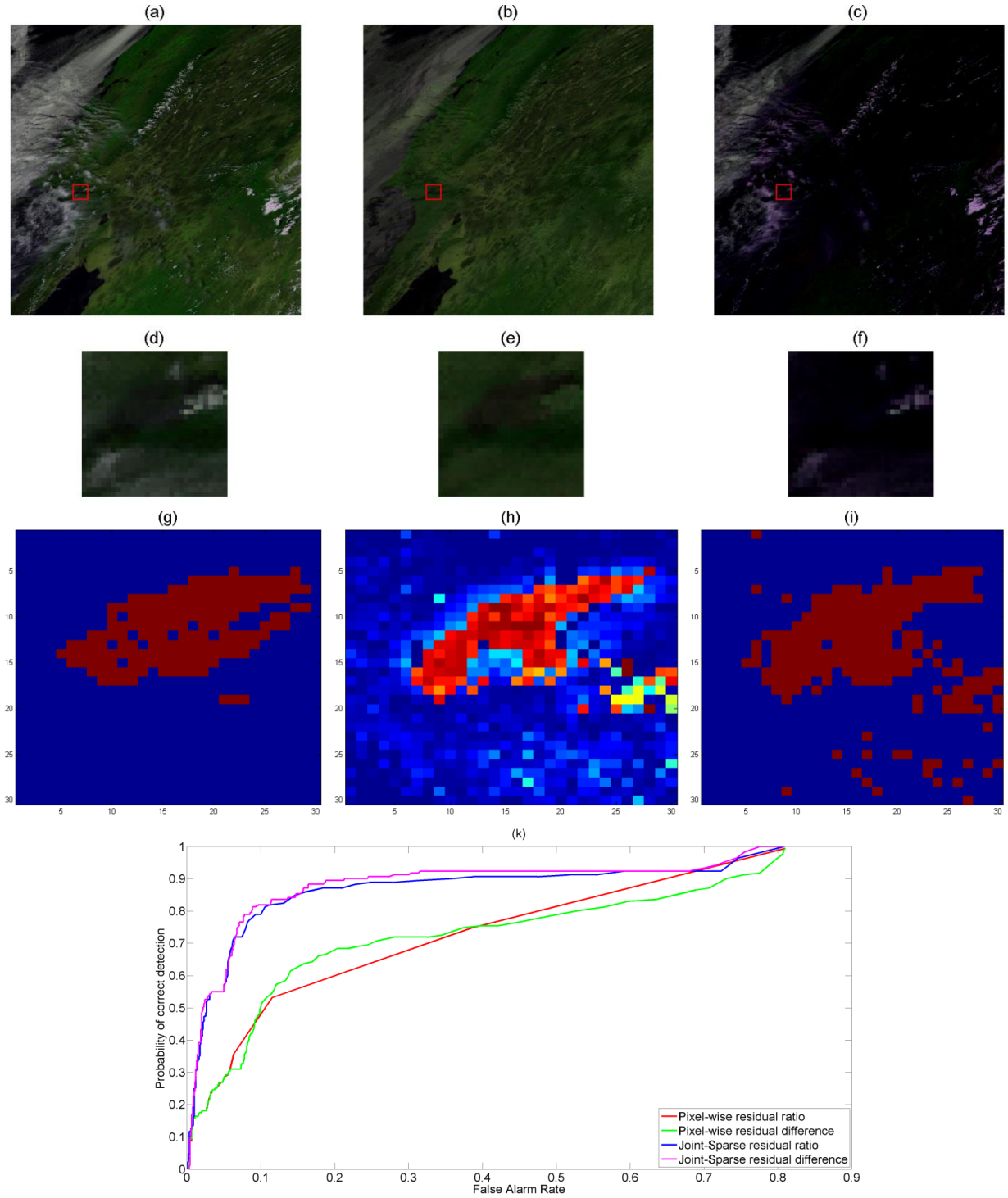

Fig. 4: Burnscar detection result for frame A2009254 (partial cloud): (a) Original HSI image in RGB mode; (b) Output low-rank component of RPCA; (c) Output sparse component of RPCA (cloud); (d) (e) and (f) Zoom-in patches of HSI images within the burnscar testing region (red-rectangle region) shown in (a), (b) and (c), respectively; (g) ground truth burn map within the testing patch; (h) Output residual difference of joint-sparsity detection; (i) Output burnscar detection (by thresholding (h)); ROC curves of pixel-wise and joint-sparsity target detections.

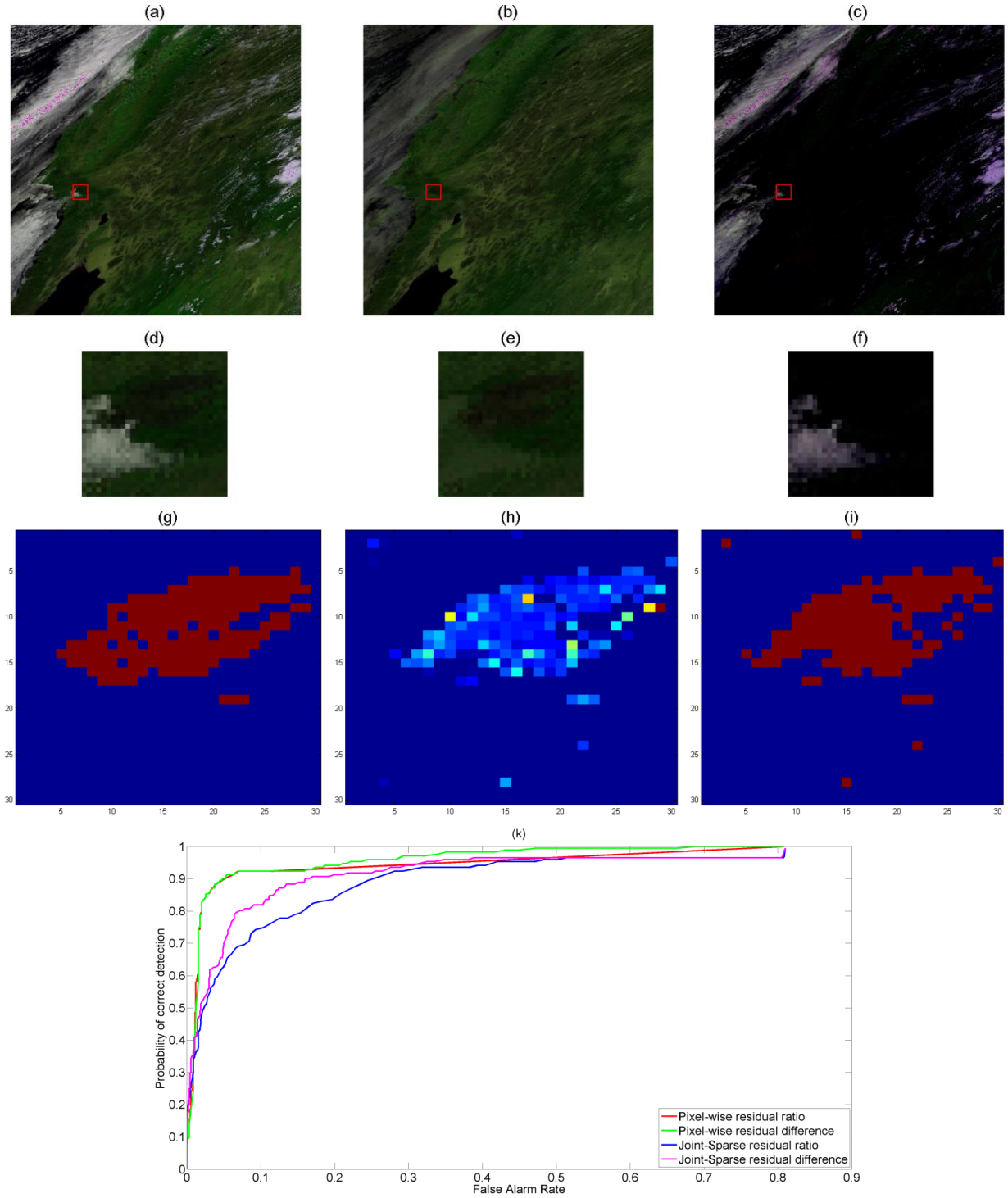

Fig. 5: Burnscar detection result for frame A2009256 (partial cloud): (a) Original HSI image in RGB mode; (b) Output low-rank component of RPCA; (c) Output sparse component of RPCA (cloud); (d) (e) and (f) Zoom-in patches of HSI images within the burnscar testing region (red-rectangle region) shown in (a), (b) and (c), respectively; (g) ground truth burn map within the testing patch; (h) Output residual difference of joint-sparsity detection; (i) Output burnscar detection (by thresholding (h)); ROC curves of pixel-wise and joint-sparsity target detections.

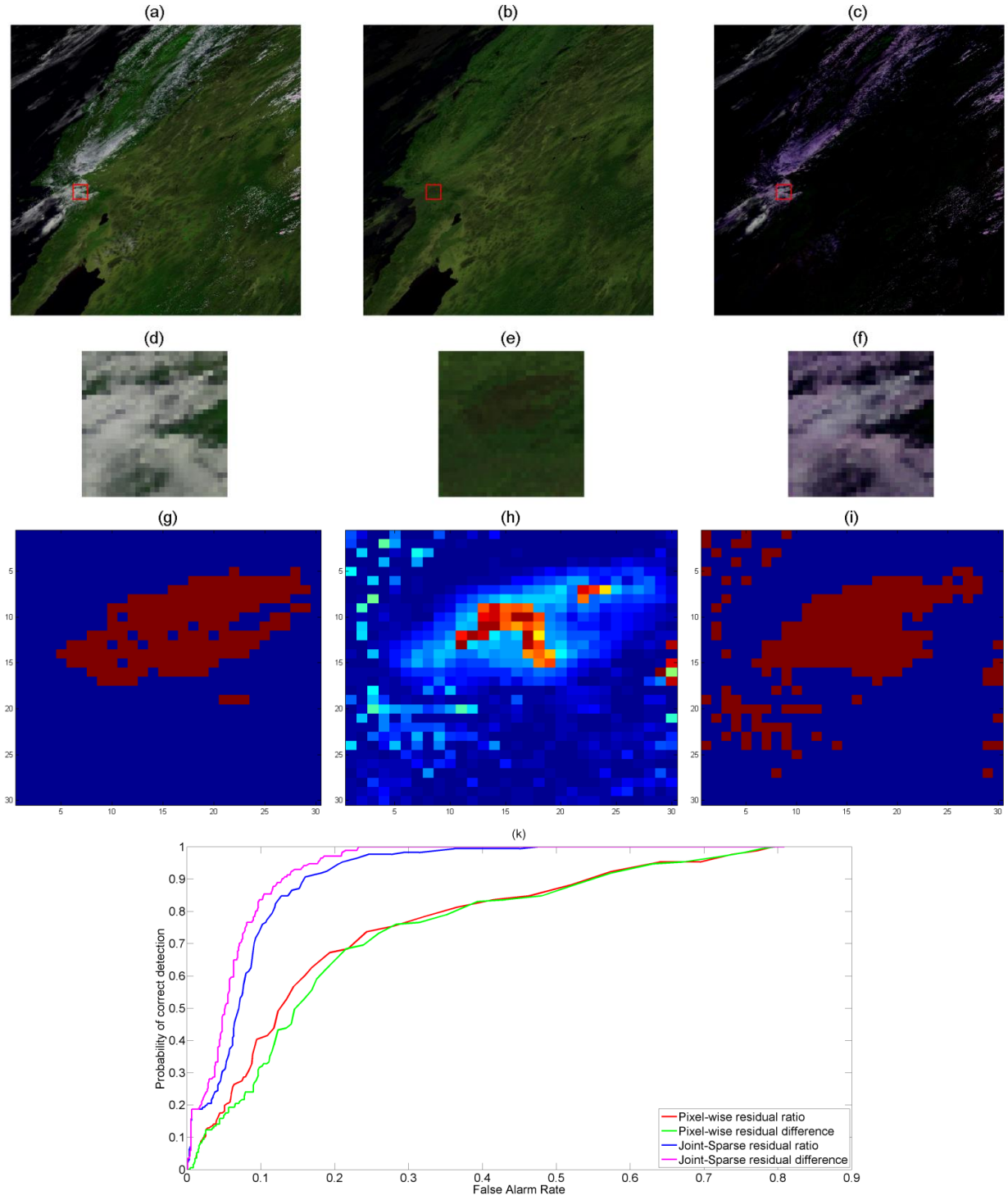

Fig. 6: Burnscar detection result for frame A2009257 (full cloud): (a) Original HSI image in RGB mode; (b) Output low-rank component of RPCA; (c) Output sparse component of RPCA (cloud); (d) (e) and (f) Zoom-in patches of HSI images within the burnscar testing region (red-rectangle region) shown in (a), (b) and (c), respectively; (g) ground truth burn map within the testing patch; (h) Output residual difference of joint-sparsity detection; (i) Output burnscar detection (by thresholding (h)); ROC curves of pixel-wise and joint-sparsity target detections.

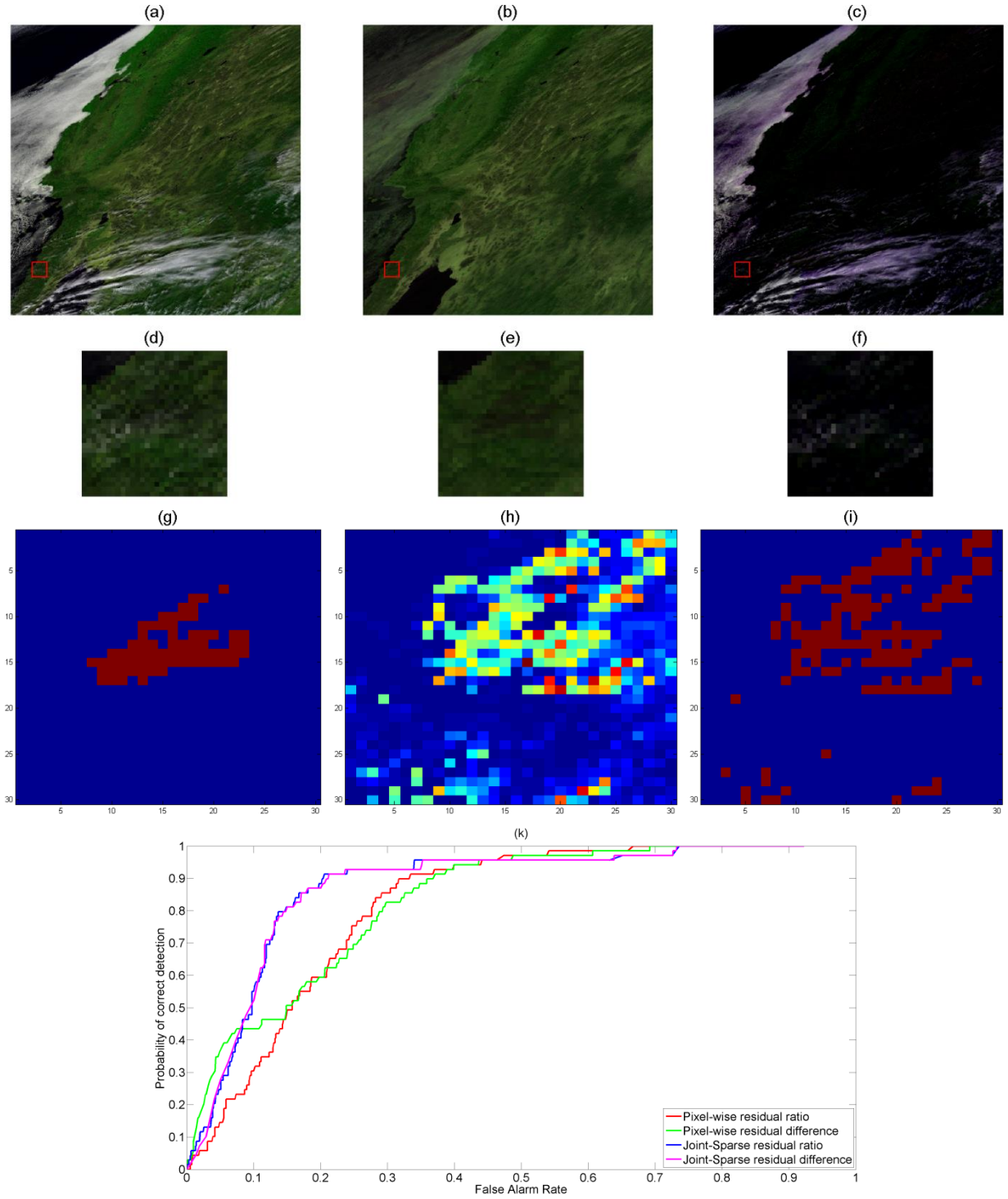

Fig. 7: Burnscar detection result for frame A2009283 (partial cloud): (a) Original HSI image in RGB mode; (b) Output low-rank component of RPCA; (c) Output sparse component of RPCA (cloud); (d) (e) and (f) Zoom-in patches of HSI images within the burnscar testing region (red-rectangle region) shown in (a), (b) and (c), respectively; (g) ground truth burn map within the testing patch; (h) Output residual difference of joint-sparsity detection; (i) Output burnscar detection (by thresholding (h)); ROC curves of pixel-wise and joint-sparsity target detections.

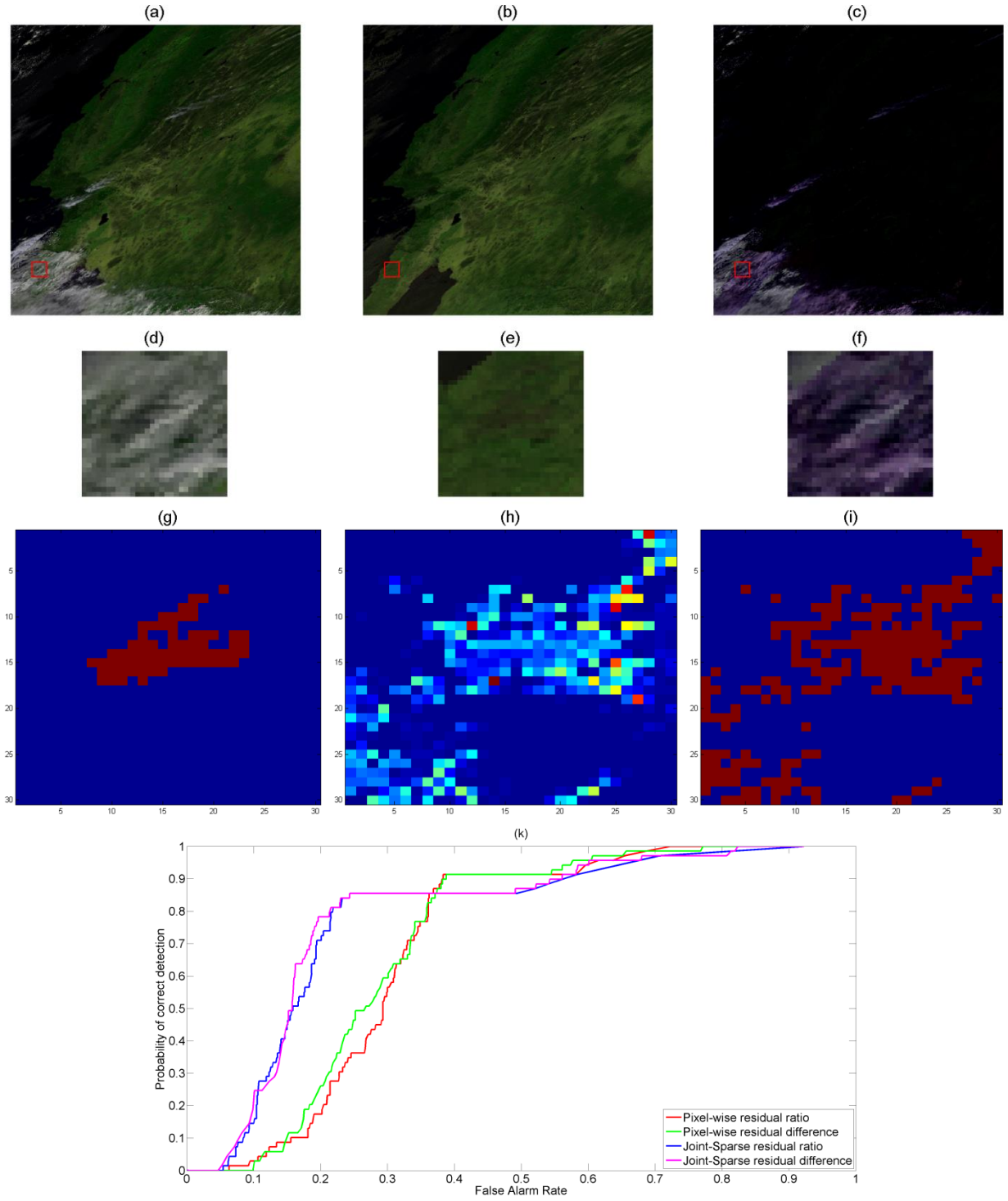

Fig. 8: Burnscar detection result for frame A2009275 (full cloud): (a) Original HSI image in RGB mode; (b) Output low-rank component of RPCA; (c) Output sparse component of RPCA (cloud); (d) (e) and (f) Zoom-in patches of HSI images within the burnscar testing region (red-rectangle region) shown in (a), (b) and (c), respectively; (g) ground truth burn map within the testing patch; (h) Output residual difference of joint-sparsity detection; (i) Output burnscar detection (by thresholding (h)); ROC curves of pixel-wise and joint-sparsity target detections.

.

4 Future Works

4.1 Robust PCA with Weighting Prior

The Robust PCA model uses a global weighting parameter λ to treat the sparse noise distribution at all locations equally. However, when we have some prior knowledge of where the noise $\boldsymbol{E}$ is more likely to appear, i.e. each element in $\boldsymbol{E}$ is appointed with a different weighting parameter representing how much assurance that element is not an outlier, we can provide better representations of the measurements by introducing a weighting matrix into the formula. The global weighting parameter λ is then replaced by a component-wise weighting matrix $\boldsymbol{W_E}$ in the cost function:

$$\min_{\boldsymbol{X},\boldsymbol{E}} \|\boldsymbol{X}\|_* + \|\boldsymbol{W_E} \circ \boldsymbol{E}\|_1 \quad s.t. \boldsymbol{Y} = \boldsymbol{X} + \boldsymbol{E}$$

where $\circ$ denotes the Hadamard (point-wise) product of two matrices.

Not only the prior information of the sparse component can be taken into account, but also the structure of the rank can be exploited to provide a better presentation of the low-rank model. The nuclear norm, by definition, can be written as the summation of all singular values $\|\boldsymbol{X}\|_* = \sum_i \sigma_i(\boldsymbol{X}) = \|\sigma(\boldsymbol{X})\|_1$ where $\sigma(\boldsymbol{X})$ is the vector of all singular values of $\boldsymbol{X}$ in the order of magnitutes from large to small. If the knowledge of the distribution of the rank can be learned in advance, the nuclear norm $\|\boldsymbol{X}\|_*$ is then altered by the weighting singular value summation $\sum_i w_{\boldsymbol{X}_i}\sigma_i(\boldsymbol{X}) = \|\boldsymbol{w_X} \circ \sigma(\boldsymbol{X})\|_1$ where $\boldsymbol{w_X}$ is the weighting vector telling how much each singular value of $\boldsymbol{X}$ should contribute to the nuclear norm. The robust low-rank matrix recovery model with weighting priors can be fully defined by the following minimization:

$$\min_{\boldsymbol{X},\boldsymbol{E}} \|\boldsymbol{w_X} \circ \sigma(\boldsymbol{X})\|_* + \|\boldsymbol{W_E} \circ \boldsymbol{E}\|_1 \quad s.t. \boldsymbol{Y} = \boldsymbol{X} + \boldsymbol{E}$$

Note that the weighting matrix $\boldsymbol{W_E}$ can be determined via a preprocessing step to detect the cloud information. This preprocessing step does not need to very precisely separate the cloud component but should provide the confident level that cloud exists or not in each pixel. One way to do this is by the general RPCA that is discussed in section 2.1. Furthermore, the singular value weighting $\boldsymbol{w_X}$ can be learned from the processing data. For example, one observation is that the rank of the background should be very small (in the idea case it is equal to the number of spectral bands in a hyperspectral frame) while burning scar may change more frequently, hence its rank should be in a larger scale.

The weighted robust matrix recovery framework (17) can be efficiently solved using the alternative direction method of multipliers (ADMM). The augmented Lagrangian function of the weighting RPCA model is expressed as:

$$\mathcal{L}(\mathbf{X}, \mathbf{E}, \mathbf{Z}) = \|\boldsymbol{w_X} \circ \sigma(\boldsymbol{X})\|_* + \|\boldsymbol{W_E} \circ \boldsymbol{E}\|_1 + \langle \boldsymbol{Y} - \boldsymbol{X} - \boldsymbol{E}, \boldsymbol{Z}\rangle + \frac{\mu}{2}\|\boldsymbol{Y} - \boldsymbol{X} - \boldsymbol{E}\|_F$$

where $\boldsymbol{Z}$ is the Lagrangian multiplier, $\mu > 0$ is a penalty parameter, $\langle\cdot,\cdot\rangle$ is the inner product and $\|\cdot\|_F$ denotes the matrix Frobenius norm. The unconstrained minimization of $\mathcal{L}(\boldsymbol{X}, \boldsymbol{E}, \boldsymbol{Z})$ can be solved by updating one variable at a time, iteratively. The detailed algorithm is summarized in algorithm 1.

Algorithm 1 Robust low-rank matrix recovery with weighting priors

Input: Data input $\mathbf{Y}$, weighting matrix $\mathbf{W_E}$, weighting vector $\mathbf{w_X}$.

1. $\mathbf{Z}_0 = 0$, $\mathbf{E}_0 = 0$, $\mu_0 > 0$, $\rho > 1$, $k = 1$
2. **While** not converged, **do**
3. $(\mathbf{U}, \mathbf{\Sigma}, \mathbf{V}) = svd(\mathbf{Y} - \mathbf{E}_k + \mu_k^{-1}\mathbf{Z}_k)$;
4. $\mathbf{X}_{k+1} = \mathbf{U}S_{\mu_k^{-1}diag(\mathbf{w_X})}[\mathbf{\Sigma}]\mathbf{V}^T$;
5. $\mathbf{E}_{k+1} = S_{\mu_k^{-1}\mathbf{W_E}}(\mathbf{Y} - \mathbf{X}_{k+1} + \mu_k^{-1}\mathbf{Z}_k)|_\Omega$
6. $\mathbf{Z}_{k+1} = \mathbf{Z}_k + \mu_k(\mathbf{Y} - \mathbf{X}_{k+1} - \mathbf{E}_{k+1})$
7. $\mu_{k+1} = \rho\mu_k$
8. $k = k + 1$
9. **end while**

where $S_\epsilon(a) = max(|a| - \epsilon, 0)\, sgn(a)$ is the element-wise soft-thresholding operator.

Outputs: $(\mathbf{X}_k, \mathbf{E}_k)$.

4.2 Joint Cloud Suppression and Burnscar Detection

We have proposed a two-step processing models to detect the burning area in hyperspectral data sets, in which the RPCA step is first processed to separate the cloud and then a spatial-temporal joint-sparsity model is conducted to detect the burnscar target using inputs as the low-rank components of the RPCA step. In the future, we want to process both step in one combined model which simultaneously suppressing the cloud and determining burning area in the same cost function. The model is proposed as follow:

$$\min_{\boldsymbol{X}} \ \|\boldsymbol{S}\|_{1,2} + \lambda_{\mathrm{L}}\|\boldsymbol{L}\|_* + \lambda_1\|\boldsymbol{E}\|_1 + \quad s.t. \boldsymbol{Y} = \boldsymbol{DS} + \boldsymbol{L} + \boldsymbol{E}$$

where $\boldsymbol{Y}$ is the original input observation, $\boldsymbol{E}$ represents the cloud information, $\boldsymbol{L}$ is the background content and $\boldsymbol{DS}$ captures the burnscar joint-sparsity representation.

Acknowledgement. This work is supported by NASA SBIR Program.

Reference

[1] E. Candes, J. Romberg, and T. Tao, "Robust uncertainty principles: Exact signal reconstruction from highly incomplete frequency information," *IEEE Trans. on Information Theory*, vol. 52, no. 2, pp. 489-509, Feb. 2006.

[2] D. L. Donoho, "Compressed sensing," *IEEE Trans. on Information Theory*, vol. 52, pp. 1289–1306, 2006.

[3] M. A. Figueiredo, R. D. Nowak, and S. J. Wright, "Gradient projection for sparse reconstruction: Application to compressed sensing and other inverse problems," *IEEE J. Sel. Topics Signal Process.*, vol. 1, no. 4, pp.586–597, Dec. 2007.

[4] E. J. Candes and B. Recht, "Exact matrix completion via convex optimization", *Foundations of Computational Mathematics*, vol. 9, pp. 717-772, 2008.

[5] E. J. Candes, X. Li, Y. Ma, and J. Wright, "Robust principal component analysis", *Journal of the ACM*, 58(3), 2011.

[6] J. Wright, A. Ganesh, S. Rao, Y. Peng, and Y. Ma, "Robust principal component analysis: Exact recovery of corrupted low-rank matrices via convex optimization," *Advances in neural information processing systems*, pp. 2080-2088, 2009.

[7] NASA Moderate Resolution Imaging Spectroradiometer Data. http://modis.gsfc.nasa.gov/data/